International Journal of Pharmaceutics 647 (2023) 123514

Contents lists available at ScienceDirect

International Journal of Pharmaceutics

journal homepage: www.elsevier.com/locate/ijpharm

Exploring the effects of high pressure on hydrogen bonding in pharmaceutical cocrystals: A systematic study of pyridine dicarboxylic acid systems using synchrotron and neutron diffraction

Martin R. Ward [a], Craig L. Bull [b,c], Nicolas P. Funnell [b], Mark R. Warren [d], Iain D.H. Oswald [a,*]

[a] Strathclyde Institute of Pharmacy and Biomedical Sciences, University of Strathclyde, 161 Cathedral Street, Glasgow G4 0RE, United Kingdom
[b] ISIS Neutron and Muon Source, Science and Technology Facilities Council, Rutherford Appleton Laboratory, Harwell Oxford, Didcot, Oxon OX11 0QX, United Kingdom
[c] Department of Chemistry, University of Edinburgh, David Brewster Road, Edinburgh EH9 3FJ, United Kingdom
[d] Diamond Light Source, Harwell Science and Innovation Campus, Didcot, Oxfordshire OX11 0DE, United Kingdom

ARTICLE INFO

Keywords:
High-pressure
Intermolecular interactions
Diffraction
X-ray
Neutron
Phase transition

ABSTRACT

Pharmaceutical cocrystals use common robust hydrogen bonding synthons to create novel materials with different physicochemical properties. In this systematic study of a series of cocrystals, we explore the effect of high pressure on one of these commonly used motifs, the acid-pyridine motif, to assess the commonality of behaviour under extreme conditions. We have surveyed five pyridine dicarboxylic acid systems using both synchrotron and neutron diffraction methods to elucidate the changes in structure. We observe that the hydrogen bonding in these systems compress at a similar rate despite the changes to the molecular make-up of the solids and that on compression the changes in structure are indicative that the layers move along the major slip planes in the structure. We have observed two phase transitions to new forms of the pyrazine:malonic acid system, one for each stoichiometric ratio. This study demonstrates that the combination of two complementary diffraction approaches is key to understanding polymorphic behaviour at high pressure.

1. Introduction

The systematic study of molecules and their derivatives is a valuable tool to understand how molecular features may impact the solid-state forms and, in turn, alter the physicochemical properties of a material (Duggirala et al., 2016). These studies have been extensively used in cocrystallisation and crystal engineering studies of active pharmaceutical ingredients (APIs) where the APIs are crystallised with a series of co-formers that are structurally related e.g. different isomers of phenyl- or pyridine-based molecules. Cocrystallisation is based on the use of robust hydrogen-bonding synthons that reproducibly interact with one another at the expense of the interactions in the pure form of the API e.g. homodimers of a carboxylic acid (Desiraju, 1995). Understanding these interactions/synthons under different thermodynamic conditions of pressure and temperature is important to provide additional information into their robustness as the materials may experience changes in their environment during materials processing.

The Cambridge Crystallographic Data Centre (CCDC) (Groom et al., 2016) curates crystallographic information on organic and metallo-organic materials in the Cambridge Structural Database (CSD) enabling researchers to extract statistically significant findings across a group of molecules. An advantage of the CSD is that it largely contains single-crystal data which is important due to the accurate molecular level detail that can be achieved. This information can then be correlated to the macroscopic properties of the solid. Recently, the CCDC have collated various subsets of compounds to allow relevant comparisons to be made using the data from the CSD. For example, the CSD Drug Subset has been cross-referenced with Drugbank 5.0 (Wishart et al., 2018) and provides a pharmaceutically relevant set of molecules. This subset contains 8635 entries of 785 unique drug molecules (at the time of publication) that can be investigated for differences in hydrogen bonding or packing behaviour (Bryant et al., 2019). Over the past 4 years this Drug Subset has grown significantly to 15 k entries (CSD2023), increasing the knowledge of how pharmaceutically relevant materials act in the solid-state.

One area that is of increasing interest to the pharmaceutical industry is high pressure. The effect of pressure on polymorphism of organic materials is well-established and is highly relevant to the

* Corresponding author.
E-mail address: iain.oswald@strath.ac.uk (I.D.H. Oswald).

https://doi.org/10.1016/j.ijpharm.2023.123514
Received 29 June 2023; Received in revised form 19 September 2023; Accepted 13 October 2023
Available online 14 October 2023

pharmaceutical industry with well-characterised materials undergoing phase transitions under tablet compaction (Wildfong et al., 2007; Thakral et al., 2019). It is imperative that these systems are probed using high-pressure to gain a better insight as to why these materials convert and what impact this might have on the future manufacturability of the material. The CCDC has recognised the increase in activity in this area and has created a High-pressure subset that can be cross-correlated with the Drug Subset to investigate the pharmaceutical materials that have been studied under pressure. By doing so, we find that only 58 pharmaceutically relevant molecules have been studied. Of particular interest to the present study of co-crystals only 27 are multi-component (salts/cocrystals) and of these only 21 contain no ions (6 possess a zwitterionic component). Despite this search being limited to the CSD, this is quite an astonishing fact given that crystal engineering, cocrystallisation and high pressure have been widely investigated for over 20 years. The reason for this could be due to the potential greater complexity of the multi-component forms over single molecule systems. Our rationale for looking into cocrystals at pressure is that they have the flexibility to form different types of hydrogen bond interactions that may not be observed in a pure compound. For example, carbamazepine is able to form homomeric amide dimers or catemers (Arlin et al., 2011; Srirambhatla et al., 2016) in the pure form but can exhibit heteromeric amide-acid dimers by the use of cocrystallisation (Childs et al., 2009; Childs et al., 2008). By using these solids we can maximise our understanding of how intermolecular interactions react under compression and relate this to their behaviour in a tabletting press. Given that there are more multicomponent forms being approved for use by the Food and Drug Administration, it is essential to understand how these materials may react under high pressure during manufacturing process.

In this paper, we have used a combination of synchrotron and neutron diffraction to investigate the effect of pressure on an archetypal hydrogen bonding motif that is used in cocrystallisation of pharmaceutical materials; the acid-pyridine interaction. As a representative model for this interaction, we focused on pyrazine and a series of dicarboxylic acids from oxalic to adipic acid (Fig. 1). Our rationale for investigating such simple systems was to minimise, as much as possible, the effects of other interactions and packing effects so that we could understand how this specific interaction is affected by pressure.

2. Material and methods

2.1. Cocrystal preparation

The cocrystals were prepared using the methodologies found in Dutkiewicz *et al.*(Dutkiewicz et al., 2015) (PYOX, PYMA 1:1, 2:1, PYGL, PYAD) and Arhangelskis *et al.*(Arhangelskis et al., 2012) (PYSU).

1:1 PYMA single crystal: Stoichiometric ratio of malonic acid and pyrazine was dissolved in acetone and the solution allowed to evaporate. On evaporation an oil was produced. A small sample of ballmilled product of the 1:1 form was added to the oil which resulted in rapid crystallization (within 30 min) of crystals suitable for single-crystal diffraction. The ball milling experiment used 250 mg of material in total in a 1:1 stoichiometric ratio. 50 μL ethanol was added so that a 0.2 μL/mg liquid/solid ratio was used. The powder was milled at 30 Hz for 30 min in 10 mL stainless steel jar with two 7 mm stainless steel milling balls.

PYAD Crystal growth: The crystal growth methods for PYAD from the literature gave very thin plate-like crystals that were not going to provide the best data once housed in a diamond anvil cell due to the weaker diffraction of the sample coupled with the higher background provided by the cell. In this instance, we used high-pressure crystal growth to anneal the crystals so that they had better quality diffraction.(Oswald and Pulham, 2008; Abbas et al., 2017; Moggach and Oswald, 2020) After the annealing process the pressure on the sample was released and the mother liquor allowed to leave the chamber. The sample chamber was refilled with petroleum ether as the pressure-transmitting medium and ruby before data collection.

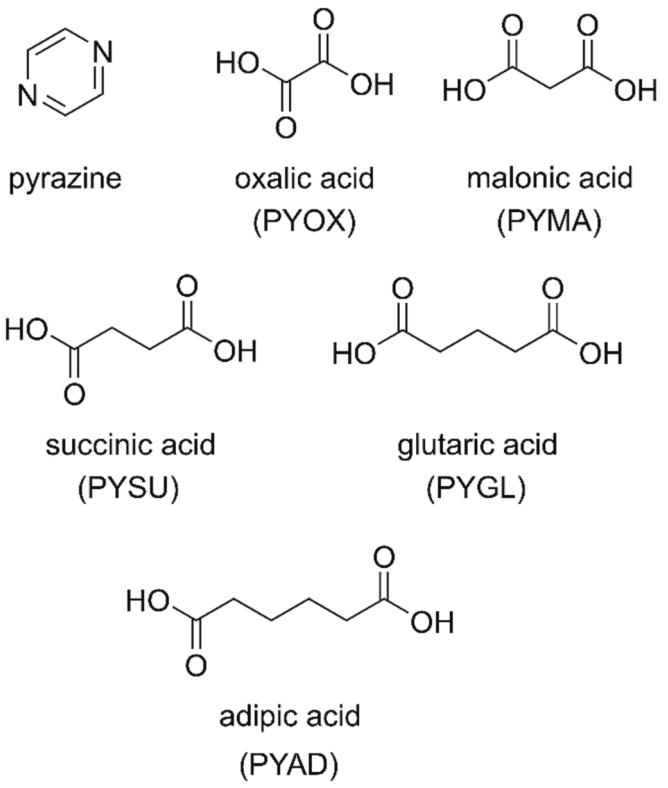

Fig. 1. Chemical diagrams of the molecules under investigation in this study. Each of the 1:1 cocrystals hydrogen bond through the OH···N interaction. The 2:1 cocrystal of malonic acid with pyrazine possess both the OH···N and OH···O interactions which adds complexity to the compression of the solids. Underneath the names of the acid is the code by which the cocrystals will be discussed herein.

2.2. Diamond anvil cell preparation

The crystals were loaded into a Merrill-Bassett Diamond Anvil Cell (DAC) modified with Boehler-Almax diamond anvils and tungsten carbide seats. The diamond culets were 600 μm in diameter and tungsten gaskets were used to house the sample. The tungsten gaskets were pre-indented from 250 μm to approximately 100 μm before a 250 μm hole was drilled in the gasket to serve as the sample chamber. Petroleum ether was used as a pressure-transmitting medium (PTM) to ensure a hydrostatic environment to 6 GPa. Ruby was used as a pressure marker following the procedures of Piermarini *et al.* (Piermarini et al., 1975).

2.3. Synchrotron and in-house data collection

Single-crystal X-ray diffraction data on the cocrystals were collected on the I19 beamline (experimental hutch 2) at Diamond Light Source, UK (Nowell et al., 2012). An X-ray wavelength of 0.4859 Å was used to enable a larger portion of reciprocal space to be accessed due to the crystals being housed in a DAC. The data were indexed and reduced using the Xia2 program (Winter, 2010) with additional multiscan absorption correction (SADABS) (Sheldrick, 2008). For PYMA 2:1 cocrystals, the data were reduced using CrystalisPro (Rigaku, 2021) and procedures therein due to the weakness of the data. Shading of the detector by the DAC was accounted for during the integration procedure.

Single crystal X-ray diffraction for PYOX was collected on in-house on a Bruker D8 Venture with a IμS Incoatec Cu (ambient pressure) or Mo (high pressure) source with a Photon II (ambient pressure) or Photon III (high pressure) CMOS detector. The final structural refinement, in all

systems, was performed in OLEX2 (Dolomanov et al., 2009) using the coordinates from the Cambridge Structural Database (CSD). Each of the cocrystal determinations possesses a unique CSD refcode; the following were used as the starting models PYOX, GUDSUV; PYMA 1:1, GUDTAC; PYMA 2:1, GUDTEG; PYGL, GUDTOQ; PYSU, VAXWAU; PYAD, GUDVAE (Groom et al., 2016). Each refinement was supported with RIGU restraints with distance restraints where necessary to ensure chemical sense of the model.

2.4. Neutron diffraction

Neutron powder diffraction data were collected on the deuterated cocrystal systems PYOX and PYMA. Deuteration was necessary to avoid the high background that is observed with hydrogenous material due to incoherent scattering from hydrogen. The data were collected on the PEARL Instrument at ISIS Neutron and Muon Source, UK (Bull et al., 2016). The ground sample was placed in a TiZr gasket with a piece of lead to act as a pressure marker and a pentane:isopentane-d_{12} (1:1 v/v) mixture as a pressure-transmitting medium. Zirconia-toughened alumina anvils were used due to their high neutron transmission, improving the signal to noise ratio. For the sample loading it was necessary to cool the anvil and gasket assembly to −10 °C in a glove bag under nitrogen gas flow to mitigate against condensation of atmospheric water. In contrast to the diamond anvil cell work, the apparatus was cooled to ensure that the PTM did not evaporate before the pressure was applied due to the increased complexity of loading. Once loaded, the anvil and gasket assembly was placed in a Paris-Edinburgh V3 press and a sealing load of 5 tonnes was applied to the gasket. Data were collected at 5 tonne steps with varying collection times. Short collection times (approx. 1 h) were used to acquire data for Pawley refinement of the unit-cell parameters, whilst longer collection times were required for Rietveld refinement against the data (4 h). Details of the collection times at each pressure are found in the ESI. The data were reduced using MANTID software (Arnold et al., 2014) to produce diffraction patterns which were corrected for the effects of the incident beam flux profile, detector efficiency, and attenuation of the beam by the anvils. Pawley and Rietveld refinements were performed in Topas Academic V5 (Coelho, 2018; Coelho, 2012). The unit-cell parameters of the sample, lead, alumina and zirconia were all refined to account for all scattering contributions to the powder pattern. Rietveld refinement of the structures was using a rigid-body description of the components allowing for overall translation and rotation of the molecules. Under high-pressure conditions it is likely that the molecular conformations change as a function of pressure however the lack of data present, due the use of the powder and optical constraints, means that the refinement of these flexible torsions are challenging.

2.5. Pixel calculations

Pixel (Gavezzotti, 2003; Gavezzotti, 2011) calculations were performed on the cocrystal systems using the MrPixel (Reeves et al., 2020) script in Mercury to provide an energetic perspective of the intermolecular interactions. Pixel requires full molecules to be able to operate i.e. Z' ≥ 1. If partial molecules are present, the symmetry needs to be reduced to provide full molecules for the calculations. For the PYOX, PYGL, and PYSU systems, Z' = 2 enabling the PixelC program to be used for the calculation of the energies directly from the structure. For PYAD, it was necessary to lower the symmetry to ensure the complete molecules. In this case, the result was two full molecules, so that PixelC calculations could be performed. For PYMA11, the symmetry had to be reduced due to the pyrazine molecules only being characterised by half a molecule due to their position relative to an inversion centre. Due to the increase in molecules, beyond Z'=2, after the reduction in symmetry, the PixelD method (dimer calculation) was used to calculate the interaction energies between pairs of molecules for the PYMA structure.

2.6. CellVol calculations

The CSD Python API code, CellVol (CwilsonEd. CellVol. Published online March 20, 2023; Wilson et al., 2022), was used to calculate the packing coefficient and void space in the crystal structures as a function of pressure. The code partitions the space in the unit cell into occupied and unoccupied volume based on the van der Waals radii of the atoms involved using a Monte Carlo procedure. From this, the molecular volume can be calculated providing a packing coefficient for the solid at each pressure point.

3. Results & discussion

3.1. Impact of compression on pyrazine:diacid systems

In this section, we discuss the impact of pressure on the pyrazine:diacid systems as model systems of a commonly occurring hydrogen bonding interaction observed in pharmaceutical products. The systems that we chose are largely made up of layered-type structures with all but PYSU showing extended layers. In addition to the 1:1 cocrystals, we have been able to isolate and study the behaviour of the 2:1 cocrystal of pyrazine and malonic acid and demonstrate how the stoichiometry alters the packing and intermolecular interactions in the system.

3.1.1. Layered structures

Oxalic, malonic, glutaric and adipic acid cocrystal systems are all based on a layered structure (Fig. 2). The difference between them is the construction of the layers. Each of the phases will be discussed briefly before considering their high-pressure behaviour collectively.

3.1.1.1. Oxalic acid (PYOX). PYOX crystallises in the monoclinic space group, Cc, with each molecule fully described by the asymmetric unit. These form two-dimensional layers primarily through the acid to pyridine interaction which is the most energetically favourable interaction in the structure (~44 kJ/mol; Table ES7). These are supplemented by weaker CH···O interactions between the hydrogen atoms of the pyrazine molecule and the oxygen atoms of neighbouring oxalic acid molecules (~16 kJ/mol; Table ES8). The intermolecular interaction energies between the layers vary from 9 to 12 kJ/mol (Table ES9) indicating a slightly weaker interaction than the intra-layer contacts.

3.1.1.2. Malonic acid (PYMA11). PYMA11 crystallises in the triclinic space group, *P*-1, with a molecule of malonic acid and two half molecules of pyrazine in the asymmetric unit. Unlike PYOX, the interaction energies between the hydrogen bonding groups are substantially different (41 kJ/mol vs 35 kJ/mol; Table ES7). This is reflected in the different hydrogen bonding distances that we observe (2.677(7) & 2.755 (5) Å; Section 3.1.1.5). The difference in energy can be explained by the orientation of the acid groups with respect to the pyrazine molecules. The stronger interaction involves the carboxylic acid and pyrazine being in the same plane whilst in the weaker interaction the acid functional group is perpendicular to the pyrazine preventing the secondary CH···O interaction being formed. Between the layers, the carboxylic acid groups of neighbouring malonic acid molecules overlap providing a significant energy contribution (15 kJ/mol; Table ES9). These interactions are supplemented by CH···O interactions between the pyrazine and malonic acid molecules (11–13 kJ/mol). On compression, this system undergoes a phase transition above 1.5 GPa to an unidentified phase restricting the comparison over a comparable pressure range (see section 3.2.2).

3.1.1.3. Glutaric acid (PYGL). PYGL possesses one molecule of pyrazine and one molecule of glutaric acid in the asymmetric unit. It crystallises in the monoclinic space group, $P2_1/n$, with the hydrogen bond linking the two molecules. These interactions are the most significant in the structure and interestingly the energy difference is ~ 10 kJ/mol

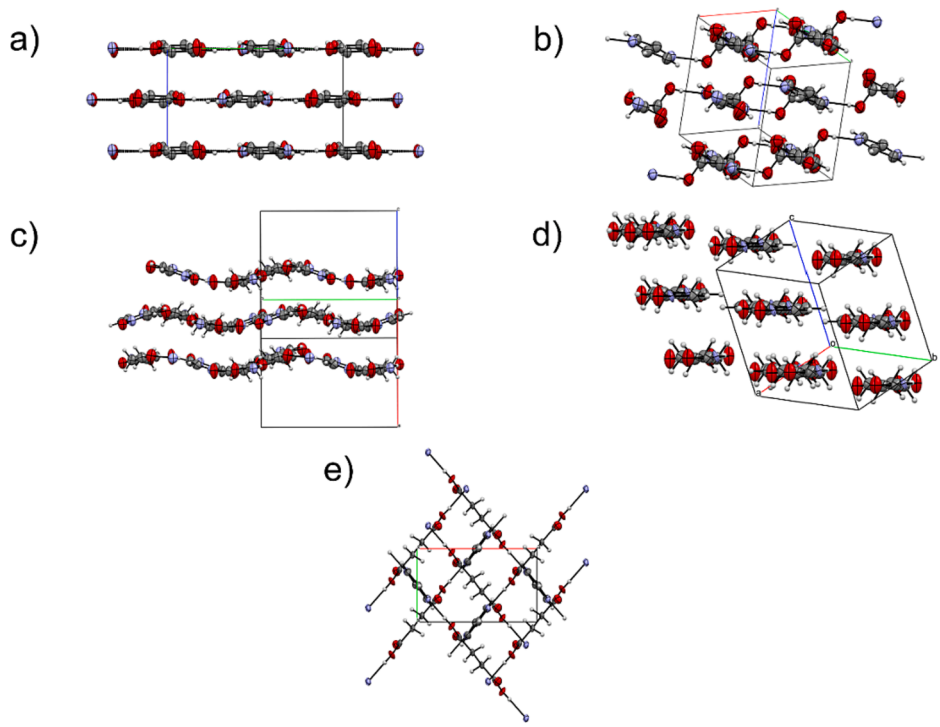

Fig. 2. Packing of the five 1:1 crystal systems explored in this investigation a) PYOX, b) PYMA11, c) PYGL, d) PYAD, e) PYSU. Note the layered nature of a-d but the change in the packing arrangement in the latter case (e).

between the two hydrogen bonds (42 vs. 32 kJ/mol; Table ES7). Whilst the difference in energy is reflected in the distances in PYMA, in this case the distances are relatively similar. There is greater overlap of the secondary CH···O interaction that helps add to the stabilisation on one interaction. The intra- and inter-layer connectivity are the next stabilising interactions with the pyrazine interacting with the oxygen atoms of glutaric acid molecule in the layer (16 kJ/mol; Table ES8) and more dispersive interaction between the glutaric acid molecules between the layers (17 kJ/mol; Table ES9).

3.1.1.4. Adipic acid (PYAD). PYAD crystallises in *P*-1 with half molecules of both pyrazine and adipic acid in the asymmetric unit. In contrast to PYGL, the energies of the hydrogen bonding interactions are equivalent in energy due to the orientation of the molecules into a $R_2^2(7)$ dimer motifs using the CH···O interactions form the pyrazine (39 & 41 kJ/mol; Table ES7). The chains are slightly offset along the *b*-direction creating a pseudo-layer through largely dispersive interactions (12–14 kJ/mol; Table ES8) and these layers stack along the *c*-direction (12–16 kJ/mol Fig. 2; Table ES9). So, whilst the spacing between the layers may be greater, the orientation of the chains enables a side-to-side overlap of the molecules hence more favourable interaction.

3.1.2. Overall compression of the layered systems

3.1.2.1. Hydrogen bonding interactions. The hydrogen bonding interaction in all the systems is the most dominant one and possesses a relatively similar strength (~40 kJ/mol) across all compounds. For the systems that require the description of two hydrogen bonds, PYOX, PYMA11 and PYGL, there is a difference in the lengths of the two bonds and consequently, there is a slight difference between the energies of interactions. PYOX shows the shortest hydrogen bonds of the series (2.660(3) & 2.645(3)Å; 49 kJ/mol). The other systems possess longer bonds that are slightly weaker in energy (40 kJ/mol) but are, nevertheless, the dominant interaction in the structure. It is important to note that Pixel energies are intermolecular energies rather than specific to a hydrogen bond hence the increased conformational flexibility in the co-former is likely to alter the intermolecular energies. The key difference in the hydrogen bonding between the systems is the differences in the interaction lengths. The simpler co-formers form shorter hydrogen bonds to the pyrazine moiety which can be related to the pKa of the acid groups (oxalic acid: 1.24 and 4.27; and malonic acid; 2.85, 5.05). Oxalic acid is known to form strong hydrogen bonds or salts easily but in this case there is no indication from the diffraction data that suggests that the salt was made in either case (Jones et al., 2012; Jones et al., 2014). Interestingly, in PYMA11, the strongest hydrogen bond follows a similar trend to the hydrogen bonds in PYOX whilst the second weaker interaction resembles distances closer to the other systems.

Despite the different lengths at ambient pressure, the compression of the hydrogen bonds across the series is consistent from 0 to 2 GPa before diverging more significantly after this pressure (Fig. 3). In general, there is a reduction in the energy between the hydrogen bonded molecules by 5–10 kJ/mol across the series. One of the observations that has come from the Pixel calculations is the stabilisation of interlayer non-directional interactions in PYMA11 and PYGL. π-interactions of the acid moieties of malonic acid aid the stabilisation of PYMA11 (5 kJ/mol) whilst the side dispersive interactions of the glutaric acid moieties (3 kJ/mol) stabilise the interaction between the layers. This highlights the need to look beyond the hydrogen bonding activity and into packing of the molecules.

3.1.2.2. Packing effects. Despite the slight change in the packing of the molecules in each of the systems studied, the compression follows a similar pattern and is strongly anisotropic where the direction of the greatest compressibility is perpendicular to the layers in the structure (Cliffe and Goodwin, 2012). The principal axes of strain (a tensor that describes the compression) for each solid is provided in Fig. S1-4 and Table S10. We have shown that in each of these solids, the energies between the layers are approximately one third of the energy observed for the main hydrogen bonding interaction but are still some of the most important in the crystal structure. These energies do not change significantly over the compression series indicating an invariant response to the change in intermolecular distance and, in fact, some intermolecular

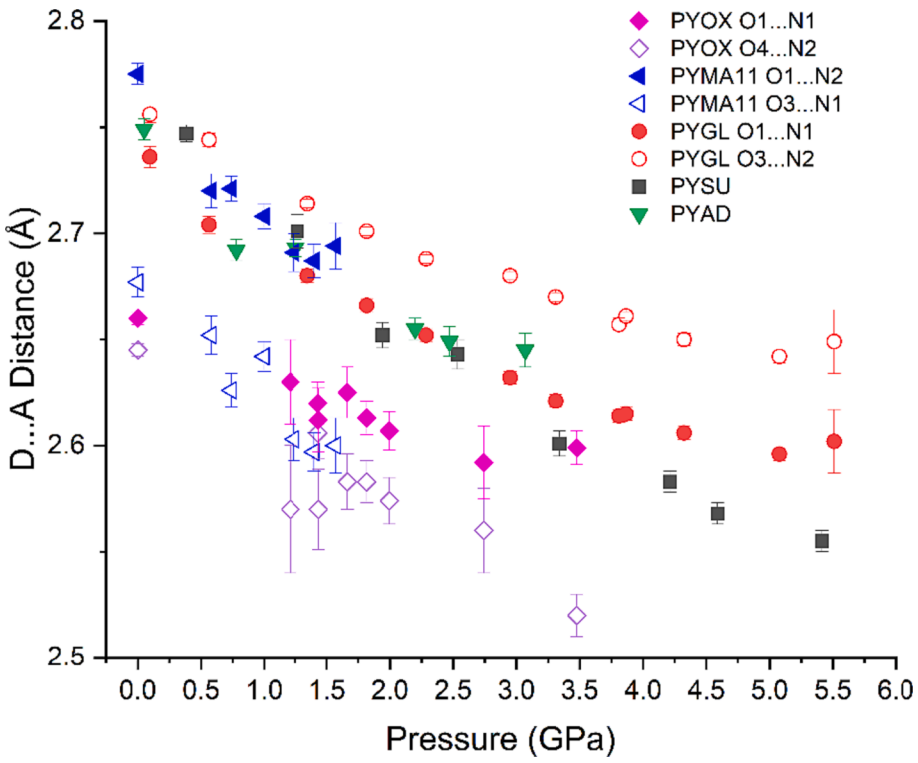

Fig. 3. The compression of the hydrogen bonds in the pyrazine:diacid systems identified using the single-crystal diffraction data. The compression of the hydrogen bonds is comparable across the systems despite the PYOX and PYMA11 systems possessing hydrogen bonds that are shorter.

interactions become more stabilising (Table S9). Therefore, there needs to be further rationale for why, despite being compressed, the interaction energies remain reasonably constant.

In the pharmaceutical literature, there has been increased attention on slip planes in a solid and the impact these have on the compaction of the material in question. In Mercury (CSD) (Macrae et al., 2008), we are able to calculate the slip planes based on the structure using the methodology of Bryant and Maloney (Bryant et al., 2018). For each of these systems, the direction of maximum compressibility corresponds to being approximately perpendicular to the slip planes present in the structure (PYOX, (0 0 2); PYMA11, (0 1 2); PYGL, (3 0—2); PYAD, (1 0—2)) which does not really provide an answer to the consistent energy over a

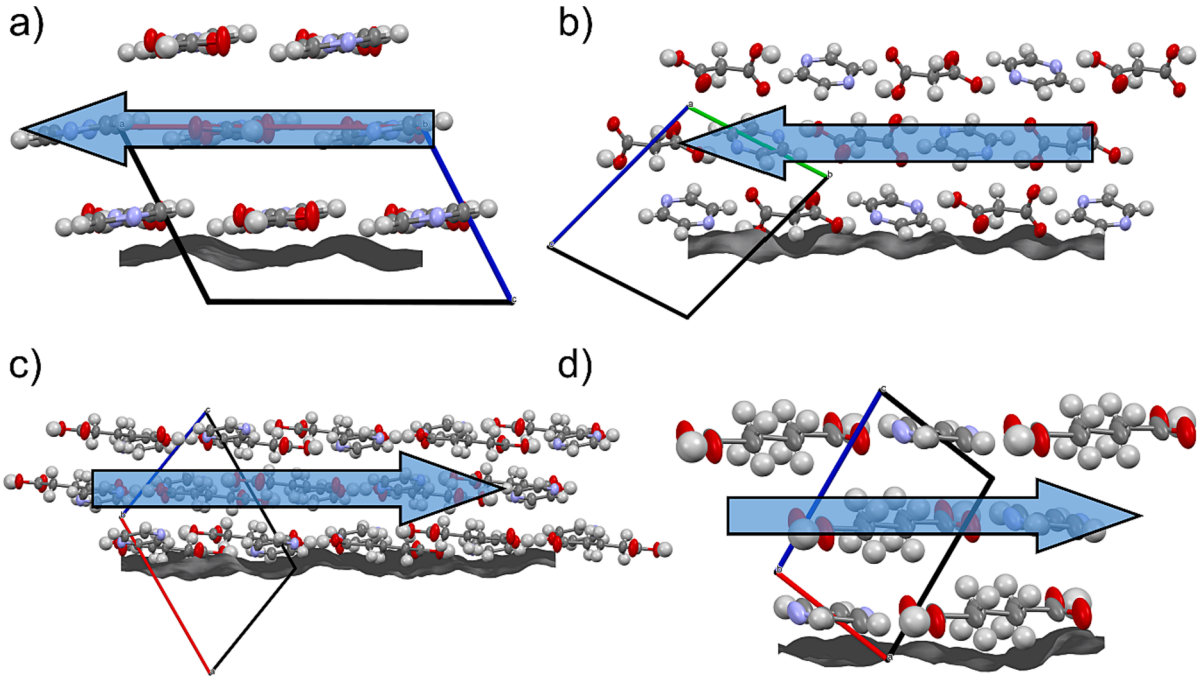

Fig. 4. The main slip planes (grey) in each of the layered systems studied a) PYOX, b), PYMA11, c) PYGL, d) PYAD. The blue arrows indicate the movement of the molecules based on the change to the unit cell angles. (For interpretation of the references to colour in this figure legend, the reader is referred to the web version of this article.)

substantial pressure range. If, however, we look in more detail at these planes and their relationship to the structure, we can see that the changes to the unit cell are commensurate with the potential slip of the layers over these surfaces. In PYOX, PYGL and PYAD, the most significant change in unit-cell angles is observed in the β-angle (for PYMA11, it is the α-angle) which would infer that the layers in the structure slip along the layer in the direction highlighted in Fig. 4. For PYOX, the β-angle increases which can be visualised by the bottom layer remaining in place but the second layer moving to the left in Fig. 4a. For PYMA11, the increase in the α-angle would be produced via the compression of the layers together but also via the layers moving in opposite directions (Fig. 4b). The decrease in the β-angle for both PYGL and PYAD can be similarly rationalised via the movement along the slip plane. So, whilst the maximum compression may be perpendicular to the defined slip planes, the structure itself moves along these planes (Fig. 4).

3.1.3. *Non-layered structure - Pyrazine:succinic acid (PYSU)*

In contrast to the other systems studied, PYSU adopts a very different packing arrangement that leads to a compression that is less anisotropic. The hydrogen bonded chains in PYSU lie approximately perpendicular to each other (77° between the mean planes of the chains) which is closely related to a wine-rack structure; a motif commonly observed in metal–organic framework materials (Fig. 5). Unlike the frameworks, there are only van der Waals interactions between the chains which enable them to act independently from one another. The intermolecular interaction energies across these layers are ~ 12 kJ/mol and this region is calculated to be one of the slip planes present in the structure (0 0 2). The two most compressible directions are observed in the *ac*-plane and are observed at an angle to the slip plane (Fig. 5a, red and blue arrows). There are large areas of void space between the hydrogen bonded chains that makes this direction compressible. Additionally, the space provides a much slower destabilisation on compression much like the layered structures. The crystal structure evolves in such a way that the β-angle increases on compression that we can equate to the slip over the (0 0 2) plane as was observed with the other systems studied. The least compressible direction is the *b*-direction that compresses the wine-rack structure. The interactions that are affected by this are the hydrogen-bonded network and the π…π interactions between the chains. Each of these interactions show a significant destabilisation on compression of 5–10 kJ/mol.

3.1.4. *Effect of component ratio (1:1 vs. 2:1) on compression in the PYMA system*

The PYMA system enables us to explore the changes in the compressibility of the solids as a function of the stoichiometric ratio of the system. The 2:1 PYMA (PYMA21) crystal structure uses both the OH···N and OH···O hydrogen bonds to build the structure (Fig. 6). Focussing on the OH···N hydrogen bond, that was common amongst the other systems studied, the length of this bond in PYMA21 is comparable to the longer bond observed in the PYMA11. The compression is smooth up to 4.3 GPa and the rate of compression of the OH···N hydrogen bond is similar to the previous systems up to 2.5 GPa before deviating to longer values equivalent to the glutaric acid system (Fig. 6). At the same time, we observe discontinuities in the OH···O interactions between 1.2 and 1.7 GPa with the hydrogen bonding elongating before further compression. This highlights the increased complexity of compression even with the addition of only one extra hydrogen bond.

To gain a better understanding of this complex system, we have used the recently-developed application, CellVol, by Wilson *et al.* (CwilsonEd. CellVol. Published online March 20, 2023; Wilson et al., 2022) It partitions the volume into void (V_{void}) and network (V_{net}) contributions (Fig. 7), presenting a more detailed understanding of how the system

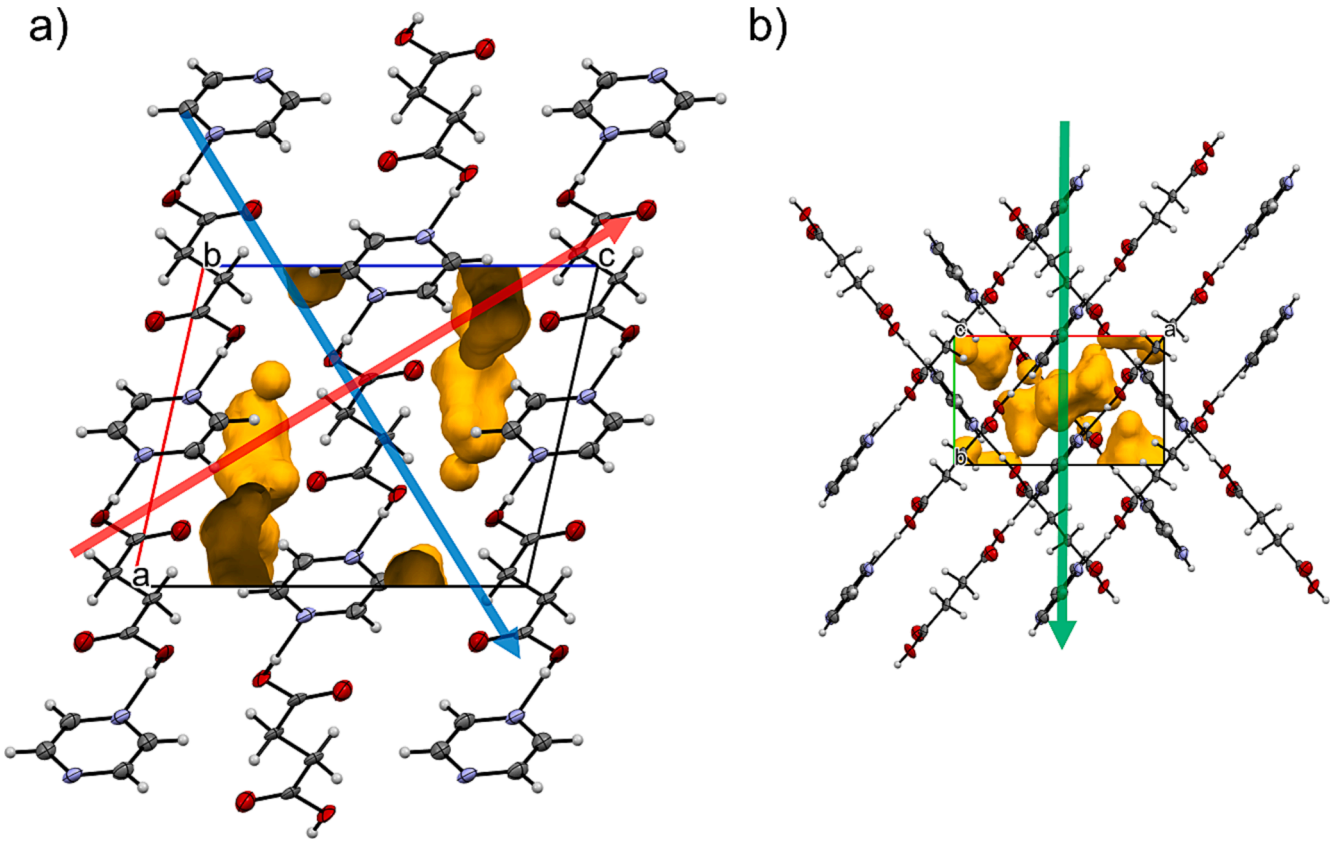

Fig. 5. The structure of PYSU viewed down the a) b-axis and b) c-axis. The structure has a layered structure that enables the direction of greatest compression (red arrow) and second greatest compression (blue arrow). The least compressible direction (green arrow) is along the b-axis and can be rationalised by the wine rack like hydrogen bonding network (b). (For interpretation of the references to colour in this figure legend, the reader is referred to the web version of this article.)

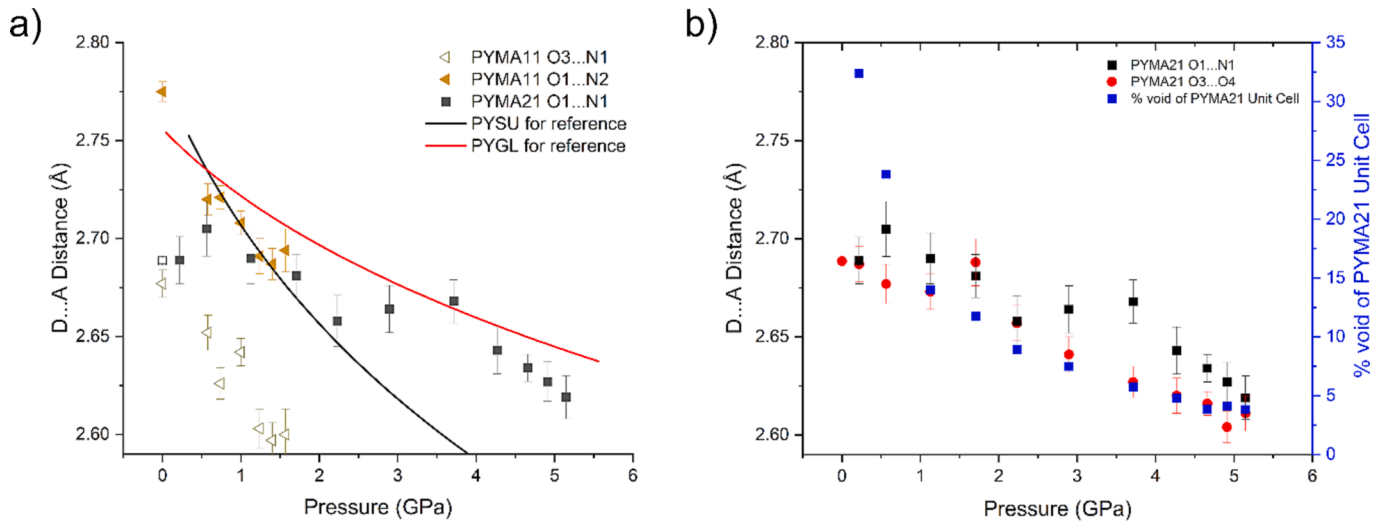

Fig. 6. A) The comparison of the hydrogen bond compression in PYMA11 (filled and hollow yellow triangles) and PYMA21 (black squares) pyrazine:malonic acid systems with reference to two other systems studied observed from the single-crystal diffraction data. b) the compression of the two hydrogen bonds present in the PYMA21 cocrystal together with the % void space in the unit cell calculated using mercury at 0.5 Å probe radius and 0.2 Å grid spacing. (For interpretation of the references to colour in this figure legend, the reader is referred to the web version of this article.)

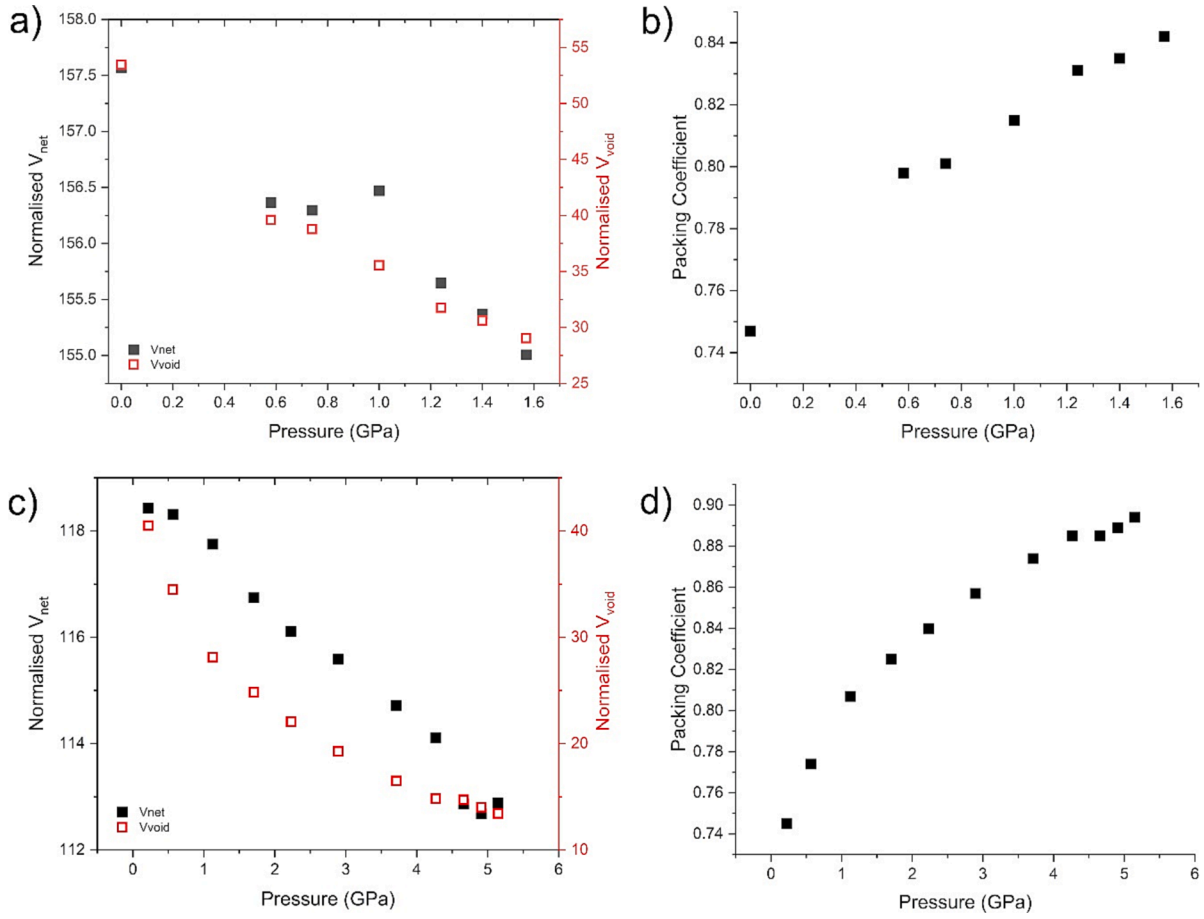

Fig. 7. The network (black squares) and void volumes (red open squares) of the PYMA11 (a) and PYMA21 (c) crystal structures calculated using the CellVol program. The combined plots of the network and void volumes (a&c) enable the correlation of the compression behaviour in these partitioned volumes. PYMA11 indicates some changes in the compression behaviour between 0.8 and 1 GPa that indicates a 2nd order phase transition. The PYMA21 system demonstrates a smooth compression of the network and void volume until 4.1 GPa before a discontinuity in these volumes indicating a change to the compression. The packing coefficients (b&d) confirm these changes. PYMA11 shows two different compression events centring around 0.8–1 GPa whilst there is a distinct reduction in the packing coefficient for the PYMA21 at 4.1 GPa. (For interpretation of the references to colour in this figure legend, the reader is referred to the web version of this article.)

accommodates the effects of pressure. Despite the changes in the individual hydrogen bonds, these do not translate to any significant variation in the compression of the network as a whole. We note that this is different to the behaviour of PYMA11 where there are changes to the compression rate in V_{net}. The calculation of V_{net} at 1 GPa seems to be larger than it should be, nevertheless, it coincides with a change in the rate of compression of the network and void volume from 0.7 GPa (Fig. 7). The hydrogen bond lengths seem to reach a limit before we observe a phase transition to a new polymorph. Unfortunately, this phase has not been identified due to the deterioration of the single crystal diffraction pattern indicating the loss of the single crystal into a powder.

The packing coefficient for the PYMA21 indicates that beyond 4.3 GPa there is a discontinuous decrease in the packing efficiency of the solid via an isostructural phase transition in the material (Fig. 7). This change is not globally observed in the unit-cell volume however it is quite clear from the packing coefficient plot that there is a change to the structure. Breaking the system down into V_{net} and V_{void} shows where the reduction occurs. The network volume reduces significantly at this pressure with some of the loss of volume taken by a slight increase in the void space. This change in distribution then allows for further compression through a reduction in void volume rather than the stiffer network volume.

In summary, all the 1:1 cocrystals investigated in this study show similar compression rates of the hydrogen-bonding interactions despite the different initial distances. The interactions become more repulsive by 5–10 kJ/mol over the pressure regime. All the systems show slip planes, and the behaviour of the unit cell compression provides evidence that the molecules do shear along this plane (within the constraints of symmetry). The compression of the 2:1 cocrystal, which possesses different hydrogen-bonding interactions, increases the complexity of the compression mechanism with the hydrogen bonds compressing at different stages. This has justified the use of such simple systems to explore the response of the carboxylic acid…pyrazine hydrogen bond to pressure. In the next section, we detail some of the practical challenges that we faced in the study and how the combination of both synchrotron and neutron diffraction enables us to study these systems more fully.

3.2. Combination of X-ray and neutron diffraction to study pharmaceutical products

The use of both X-ray single-crystal synchrotron and neutron-powder diffraction is a powerful combination of techniques that can help expand our understanding of crystal structures in a wide phase space. In this study, there were two systems that exhibited behaviour that we believe is worthwhile highlighting as they have also been observed for pharmaceutical materials under high pressure conditions. The PYOX and PYMA21 systems demonstrate: potential degradation of the crystal due to the intensity of synchrotron radiation; and potential particle size-dependent phase transformations.

3.2.1. Potential degradation by synchrotron radiation

The first system to discuss is the PYOX system. Our initial investigation using X-rays was curtailed at approx. 2 GPa due to a significant deterioration in the single-crystal diffraction pattern with reflection profiles becoming elongated at this pressure. There was still diffraction intensity present however the poor quality of the single crystal prohibited any further investigation. This change indicated that either the solid was being damaged by the synchrotron beam (Bogdanov et al., 2021; Collings and Hanfland, 2022; Meents et al., 2009) or that the material itself was undergoing a reconstructive phase transition at this pressure; both problems could be resolved with the aid of neutron powder diffraction. Neutrons are far less damaging to samples and they have been successfully employed to explore organic systems that may be susceptible to radiation damage (acrylic acid) (Oswald and Urquhart, 2011; Johnston et al., 2014). Secondly, if the solid was beginning to undergo a reconstructive phase transition, where the single crystal breaks up into a powder, then the powder diffraction element would enable us to continue the structural investigation.

From the neutron diffraction measurements (Fig. 8a), we observe that the PYOX system remains in the same phase despite our initial observations using the single crystal. There is a smooth compression of the crystal structure up to 4.6 GPa which was the highest pressure achieved. From these data, the unit-cell parameters were obtained using Pawley and Rietveld refinements (Fig. 8b-f). Two compression cycles were made with separate loadings to verify that the sample did not change phase but the unit-cell parameters of both of these compression cycles map onto one another very well. We also performed further single-crystal X-ray diffraction measurements on a laboratory source based on our observations from the neutron powder diffraction experiment at PEARL. These data also fit well with the neutron data which indicates the deterioration of the pattern is likely to be the instability of the cocrystal in the synchrotron X-ray beam.

3.2.2. Particle size-dependent phase transformations

The second neutron diffraction study was of PYMA21 to correlate with the information from the single-crystal X-ray diffraction experiments (Section 3.1.4). Interestingly, on compression of the powder beyond 1 GPa the diffraction pattern significantly altered indicating the change to a new solid form (Fig. 9a). This was not observed from the single-crystal work that was conducted at Diamond Light Source. This was a surprising observation as the diffraction from the single crystal of the PYMA21 was consistently good throughout the pressure range without any change in the crystal structure or deterioration in the pattern as one might expect from a phase transition. This indicated that either the mode of compression (hydrostatic or non-hydrostatic), particle size or the kinetics of the transition altered the behaviour of the solid (Wildfong et al., 2007; Fisch et al., 2015). There is no indication of a change to a non-hydrostatic compression regime as indicated by the consistency of the refined unit-cell parameters and the peak shapes from the neutron powder diffraction and the single crystal experiments (Fig. 9b). Therefore, it is likely that this is related either to the particle size i.e. single crystal vs powder, or the experimental time.

The main differences between the synchrotron and neutron work in this study are: the sample scattering size; rate of compression; and the measurement time. The sample volumes are not necessarily important in themselves but the ratio of solid to liquid (PTM) can increase the interfacial area between the sample and liquid thereby potentially promoting the conversion between phases. The rate of compression applied by the Paris-Edinburgh press was much slower than the DAC experiments. The pressure increases in the DAC were 0.5–1 GPa steps in a matter of seconds before stabilisation compared with the application over minutes using the relatively large volume Paris-Edinburgh press assembly (Bull et al., 2016). This controlled compression can facilitate the observation of high-pressure phases by preventing super-compression of phase beyond their thermodynamically stable region (Eikeland et al., 2016; Eikeland et al., 2017; Paliwoda et al., 2012). The last factor is the data collection times where the differences are substantial. For neutron diffraction, the collection times are much longer due to the interactions of the neutrons with the solid. In general, neutron powder diffraction measurements can take at least 15 min to collect, but usually an hour for a sufficient signal-to-noise ratio for Pawley refinement but can be around 4 h for a diffraction pattern that can be used for Rietveld refinement (*cf.* 3 min for synchrotron powder or 20 min for single crystal synchrotron measurements). These three factors are a source of variability been the techniques and potentially the solid-state behaviour of the sample.

To rationalise the differences in the behaviour observed between the synchrotron and neutron studies, we loaded a single-crystal sample into a DAC to mimic the time taken for the neutron experiment. During this investigation, single crystals did not show any visual change on compression but when the sample was decompressed, the crystal

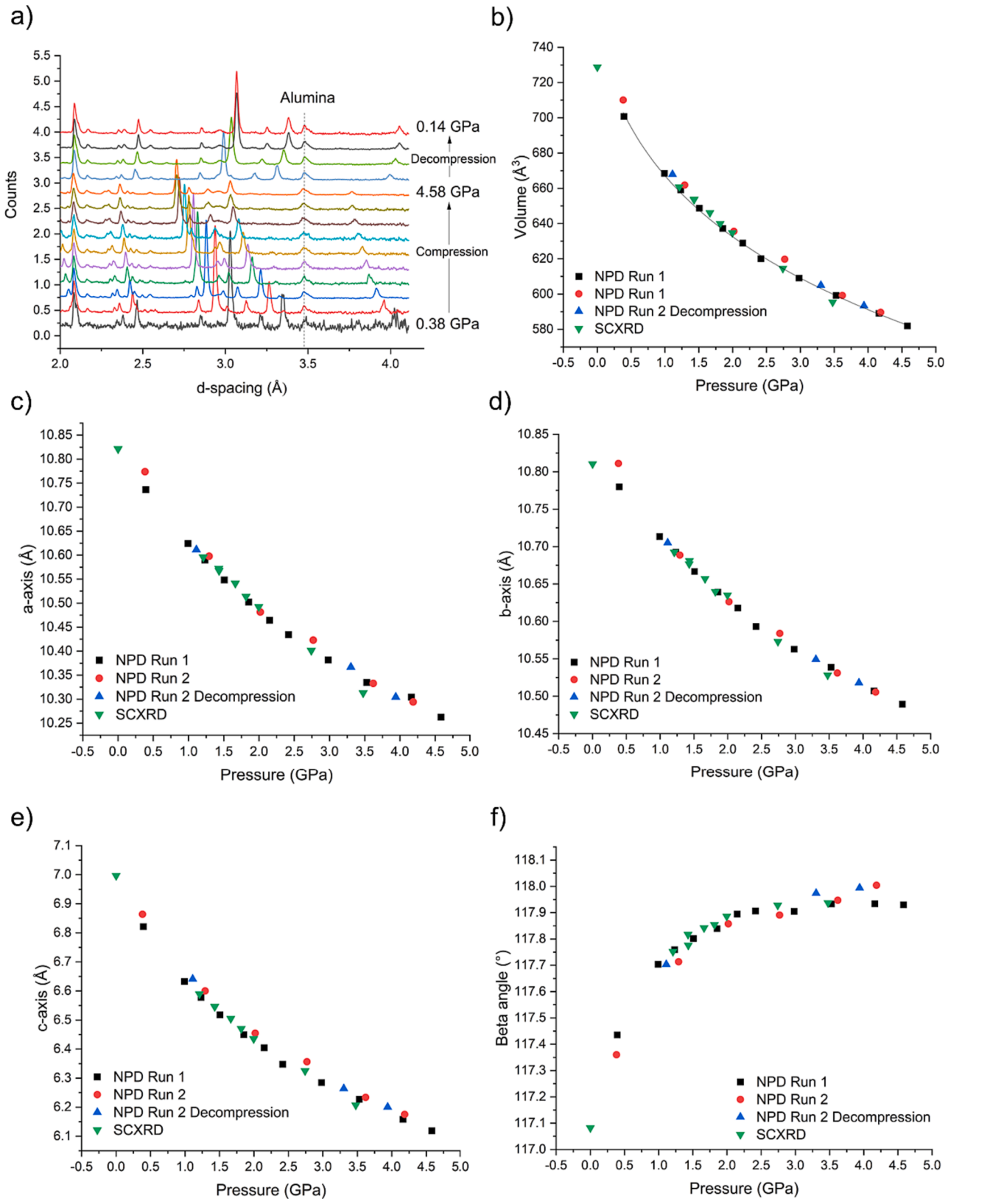

Fig. 8. (a) Neutron-diffraction data obtained during compression of PYOX up to 4.58 GPa and subsequent decompression back to ambient pressure. A contaminant alumina peak (part of the Paris-Edinburgh Press assembly) is highlighted due to its relative invariance with pressure. There is a smooth compression over the entire pressure range indicating the stability of the ambient pressure phase to pressure. (b-f) The unit cell parameters obtained from the fit of the unit cell parameters using Pawley and Rietveld refinement using two separate powder diffraction runs and a single crystal dataset. The line represents the Equation of State using the 1st run from neutron powder diffraction data (3rd-Order Birch-Murnaghan; $V_0 = 749(15)$ Å^3;K_0 3(2) GPa; K' 17(7)).

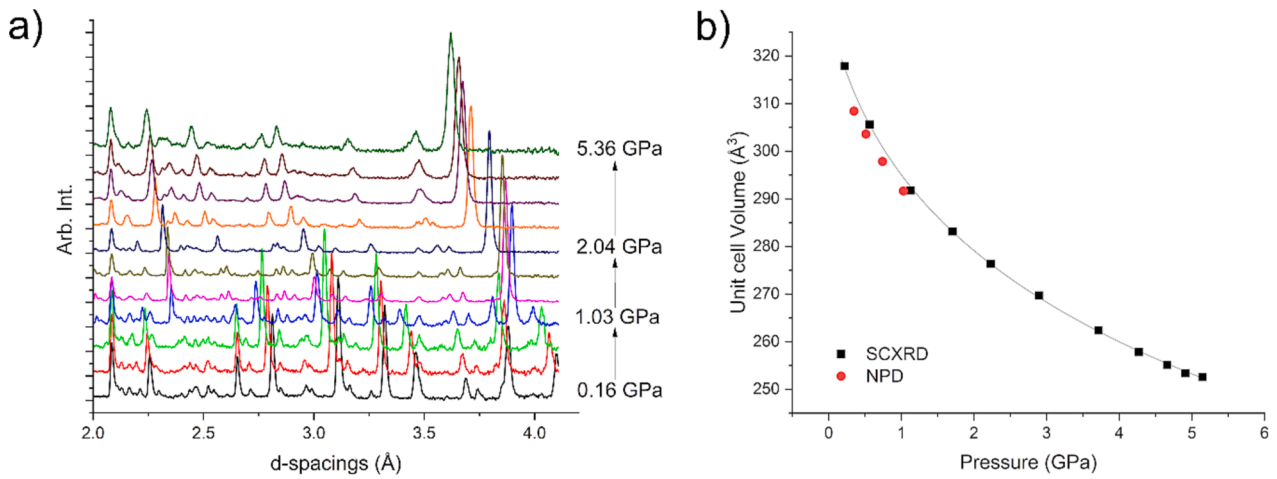

Fig. 9. (a) Neutron-diffraction data obtained during compression of PYMA21 up to 5.75 GPa and subsequent decompression back to ambient pressure. The limit of compression is highlighted by the blue dashed line and blue asterisk. During compression a phase transition between 0.75 and 1.03 GPa was observed,. (b) Pawley refinement of the diffraction data show a smooth compression of the PYMA21 phase before the transition. The line represents the Equation of State using the 1st run from Neutron Powder diffraction data (3rd-Order Birch-Murnaghan; $V_0 = 329(4)$ Å^3;K_0 4.6(15); K' 13(4)). (For interpretation of the references to colour in this figure legend, the reader is referred to the web version of this article.)

became opaque indicating a change to the solid via a reconstructive phase transition. This observation together with the neutron powder diffraction results suggests that this phase is the most thermodynamically stable above 1 GPa but without determining the structure, this cannot be confirmed. This demonstrates one of the important observations of high-pressure research, that phase boundaries can be ill-defined due to the supercompression of phases i.e. compression beyond the thermodynamic boundary between phases. It is only on decompression (or slow compression) that phase transitions to new unidentified phase are observed. Resorcinol is one such example where the ambient α-phase is retained on rapid compression (Rao et al., 2002). However it has been recently shown by Safari and Katrusiak that the observation of the higher pressure phase was suppressed due to kinetics of the experiment (Safari and Katrusiak, 2021). Serine has also been subject to kinetic studies at pressure (Fisch et al., 2015). Unfortunately, in this case, we have been unable to index the new high-pressure form of the PYMA21 cocrystal despite our best efforts. The range of *d*-spacing observable is limited by the instrumental parameters such as the time-of-flight range and angle of the detectors and also the geometry of the Paris-Edinburgh press (Bull et al., 2016) hence it has proved too challenging to solve the structure. This has prevented a more detailed structural analysis that would have shed light on why the phase transition occurred.

4. Conclusions

This work has begun to explore structural systematics in cocrystalline materials under high pressure conditions. Although it is an area that has been largely unexplored, it holds great significance in terms of utilizing crystal engineering techniques for pharmaceuticals across various thermodynamic conditions, to discover new solid-state forms of APIs. From a structural perspective, the compression in all the layered systems shows a similar anisotropic compression. At the intermolecular interaction level, we have found that the rate of compression for the acid/pyridine hydrogen bond is similar across the systems studied despite any changes in the initial hydrogen bond length. We have observed that the movement of the molecules on compression can be correlated with the slip plane in the materials where we observe the slip of one layer over another consistently across the systems studied.

Both the 1:1 and 2:1 PYMA system display phase transformations. Whilst the single crystal of the 1:1 deteriorates on compression, the 2:1 single crystal can be supercompressed beyond the phase boundary; the transition is only observed in the powdered sample. This change in behaviour depending on crystallite size is an important and common occurrence in organic materials. The ambient phase can be supercompressed beyond the boundary into a metastable region of the pressure/temperature phase diagram. This can provide a false sense of security that there are no further phases at high pressures whilst thermodynamically there may be further stable phases at pressure. Kinetic effects are an under evaluated factor at high pressure but they are of critical significance for APIs.

From a methodological viewpoint, the pyrazine:diacid systems have allowed us to investigate changes in hydrogen bonding without the influence of substituents on the behaviour of solids. Combining synchrotron and neutron measurements has revealed pressure-dependent changes in these systems. Synchrotron radiation provides the rapid data collection times (<30 mins per collection) and opens up the possibility of structural systematics such as those in this article. The utilization of neutron diffraction offers several benefits, including non-destructive alternative to an intense synchrotron X-ray beam, increased sample (& scattering) size when used in conjunction with the Paris-Edinburgh press which allows for improved powder averaging thereby enhancing the quality of data. As a result, more precise intensities can be obtained for Rietveld refinement of crystal structures. From the perspective of studying pharmaceutical materials, in either sample environment, we showed that particle size (single crystal vs powder) can have an impact on the observation of phases. Factors such as the solid–liquid ratio and increased sample surface area are integral to the procedure therefore consideration of these are important if high pressure is being used as a crystal structure screening tool for pharmaceutical materials. While high-pressure powder diffraction may not be easy to achieve in a lab setting, using both powder and single crystals can provide a more comprehensive view of the system being studied.

Declaration of Competing Interest

The authors declare the following financial interests/personal relationships which may be considered as potential competing interests: Iain D H Oswald reports financial support was provided by Engineering and Physical Sciences Research Council. Iain D H Oswald reports financial support was provided by Science and Technology Facilities Council. Iain D H Oswald reports a relationship with Science and Technology Facilities Council that includes: board membership, consulting or advisory, and travel reimbursement.

Data availability

The data will be made available via a DOI link to our Pure system. The raw neutron data is available via the DOI in the manuscript

Acknowledgements

The authors would like to acknowledge Simon Parsons, Jacob Shephard, Helen Duncan, Giulia Novelli from University of Edinburgh for their help in data collection during the Block Allocation Group (MT16169) at Diamond Light Source. We thank Andy Maloney (CCDC) for help in defining the search criterion of the Cambridge Structural Database. CCDC deposition numbers 2267853-2267905.

Funding: This work was supported by the EPSRC for funding (IDHO & MRW EP/N015401-1), Diamond Light Source (MT16169), Science and Technology Facilities Council (RB2010054). The authors would like to acknowledge that all data underpinning the characterization of the solid forms are openly available from the University of Strathclyde KnowledgeBase (https://doi.org/10.15129/5f78c84f-9d85-4d63-ad0e-dbc7f4173ea9). The raw neutron data can be accessed at doi:10.5286/ISIS.E.RB2010054

Appendix A. Supplementary data

Supplementary data to this article can be found online at https://doi.org/10.1016/j.ijpharm.2023.123514.

References

Abbas, N., Oswald, I.D.H., Pulham, C.R., 2017. Accessing mefenamic acid form ii through high-pressure recrystallisation. Pharmaceutics 9 (4), e16.

Arhangelskis, M., Lloyd, G.O., Jones, W., 2012. Mechanochemical synthesis of pyrazine: dicarboxylic acid cocrystals and a study of dissociation by quantitative phase analysis. CrystEngComm 14 (16), 5203–5208. https://doi.org/10.1039/C2CE25121C.

Arlin, J.B., Price, L.S., Price, S.L., et al., 2011. A strategy for producing predicted polymorphs: catemeric carbamazepine form V. Chem. Commun. 47 (25), 7074. https://doi.org/10.1039/c1cc11634g.

Arnold, O., Bilheux, J.C., Borreguero, J.M., et al., 2014. Mantid—Data analysis and visualization package for neutron scattering and μ SR experiments. Nucl. Instrum. Methods Phys. Res., Sect. A 764, 156–166. https://doi.org/10.1016/J.NIMA.2014.07.029.

Bogdanov, N.E., Zakharov, B.A., Chernyshov, D., Pattison, P., Boldyreva, E.V., 2021. Phase transition in an organic ferroelectric: glycinium phosphite, with and without X-ray radiation damage. Acta Cryst. B. 77 (3), 365–370. https://doi.org/10.1107/S2052520621003127.

Bryant, M.J., Maloney, A.G.P., Sykes, R.A., 2018. Predicting mechanical properties of crystalline materials through topological analysis. CrystEngComm 20 (19), 2698–2704. https://doi.org/10.1039/c8ce00454d.

Bryant, M.J., Black, S.N., Blade, H., Docherty, R., Maloney, A.G.P., Taylor, S.C., 2019. The CSD drug subset: the changing chemistry and crystallography of small molecule pharmaceuticals. J. Pharm. Sci. 108 (5), 1655–1662. https://doi.org/10.1016/j.xphs.2018.12.011.

Bull, C.L., Funnell, N.P., Tucker, M.G., Hull, S., Francis, D.J., Marshall, W.G., 2016. PEARL: the high pressure neutron powder diffractometer at ISIS. High Press Res 36 (4), 493–511. https://doi.org/10.1080/08957959.2016.1214730.

Childs, S.L., Rodríguez-Hornedo, N., Reddy, L.S., et al., 2008. Screening strategies based on solubility and solution composition generate pharmaceutically acceptable cocrystals of carbamazepine. CrystEngComm 10 (7), 856–864. https://doi.org/10.1039/B715396A.

Childs, S.L., Wood, P.A., Rodríguez-Hornedo, N., Reddy, L.S., Hardcastle, K.I., 2009. Analysis of 50 crystal structures containing carbamazepine using the materials module of mercury CSD. Cryst. Growth Des. 9 (4), 1869–1888. https://doi.org/10.1021/cg801056c.

Cliffe, M.J., Goodwin, A.L., 2012. PASCal: A principal axis strain calculator for thermal expansion and compressibility determination. J. Appl. Cryst. 45 (6), 1321–1329. https://doi.org/10.1107/S0021889812043026.

Coelho, A.A., 2018. TOPAS and TOPAS-Academic: An optimization program integrating computer algebra and crystallographic objects written in C++. J. Appl. Cryst. 51 (1), 210–218. https://doi.org/10.1107/S1600576718000183.

Coelho A. TOPAS – Academic: General Profile and Structure Analysis Software for Powder Diffraction Data. *TOPAS – Academic: General Profile and Structure Analysis Software for Powder Diffraction Data*. Published online 2012.

Collings, I.E., Hanfland, M., 2022. Effect of synchrotron X-ray radiation damage on phase transitions in coordination polymers at high pressure. Acta Cryst. B 78 (2), 100–106. https://doi.org/10.1107/S2052520622001305.

CwilsonEd. CellVol. Published online March 20, 2023. Accessed March 22, 2023. https://github.com/CwilsonEd/CellVol.

Desiraju, G.R., 1995. Supramolecular synthons in crystal engineering—a new organic synthesis. Angew. Chem. Int. Ed. Eng. 34 (21), 2311–2327. https://doi.org/10.1002/anie.199523111.

Dolomanov, O.V., Bourhis, L.J., Gildea, R.J., Howard, J.A.K., Puschmann, H., 2009. OLEX2: a complete structure solution, refinement and analysis program. J. Appl. Cryst. 42 (2), 339–341. https://doi.org/10.1107/S0021889808042726.

Duggirala, N.K., Perry, M.L., Almarsson, O., Zaworotko, M.J., 2016. Pharmaceutical cocrystals: along the path to improved medicines. Chem. Commun. 52 (4), 640–655. https://doi.org/10.1039/C5CC08216A.

Dutkiewicz, G., Dutkiewicz, E., Kubicki, M., 2015. Even–odd effect in the co-crystals of pyrazine and dicarboxylic acids. Struct. Chem. 26 (1), 247–259. https://doi.org/10.1007/s11224-014-0478-3.

Eikeland, E., Thomsen, M.K., Madsen, S.R., Overgaard, J., Spackman, M.A., Iversen, B.B., 2016. Structural collapse of the hydroquinone-formic acid clathrate: a pressure-medium-dependent phase transition. Chem. A Eur. J. 22 (12), 4061–4069. https://doi.org/10.1002/chem.201504908.

Eikeland, E., Thomsen, M.K., Overgaard, J., Spackman, M.A., Iversen, B.B., 2017. Intermolecular interaction energies in hydroquinone clathrates at high pressure. Cryst. Growth Des. 17 (7), 3834–3846. https://doi.org/10.1021/acs.cgd.7b00408.

Fisch, M., Lanza, A., Boldyreva, E., Macchi, P., Casati, N., 2015. Kinetic control of high-pressure solid-state phase transitions: a case study on l -serine. J. Phys. Chem. C 119 (32), 18611–18617. https://doi.org/10.1021/acs.jpcc.5b05838.

Gavezzotti, A., 2003. Calculation of intermolecular interaction energies by direct numerical integration over electron densities. 2. An improved polarization model and the evaluation of dispersion and repulsion energies. J. Phys. Chem. B 107 (10), 2344–2353. https://doi.org/10.1021/Jp022288f.

Gavezzotti, A., 2011. Efficient computer modeling of organic materials. The atom-atom, Coulomb-London-Pauli (AA-CLP) model for intermolecular electrostatic-polarization, dispersion and repulsion energies. New J. Chem. 35 (7), 1360–1368. https://doi.org/10.1039/C0NJ00982B.

Groom, C.R., Bruno, I.J., Lightfoot, M.P., Ward, S.C., 2016. The cambridge structural database. Acta Cryst. B72, 171–179. https://doi.org/10.1107/S2052520616003954.

Johnston, B.F., Marshall, W.G., Parsons, S., Urquhart, A.J., Oswald, I.D.H., 2014. Investigation of acrylic acid at high pressure using neutron diffraction. J. Phys. Chem. B 118 (14), 4044–4051. https://doi.org/10.1021/jp502095n.

Jones, A.O.F., Lemée-Cailleau, M.H., Martins, D.M.S., et al., 2012. Temperature dependent solid-state proton migration in dimethylurea-oxalic acid complexes. Phys. Chem. Chem. Phys. 14 (38), 13273–13283. https://doi.org/10.1039/c2cp41782k.

Jones, A.O.F., Leech, C.K., McIntyre, G.J., Wilson, C.C., Thomas, L.H., 2014. Engineering short, strong hydrogen bonds in urea di-carboxylic acid complexes. CrystEngComm 16 (35), 8177–8184. https://doi.org/10.1039/C4CE00587B.

Macrae, C.F., Bruno, I.J., Chisholm, J.A., et al., 2008. Mercury CSD 2.0 - new features for the visualization and investigation of crystal structures. J. Appl. Cryst. 41 (2), 466–470. https://doi.org/10.1107/S0021889807067908.

Meents, A., Dittrich, B., Gutmann, S., 2009. A new aspect of specific radiation damage: hydrogen abstraction from organic molecules. J. Synchrotron Radiat. 16 (2), 183–190. https://doi.org/10.1107/S0909049509002192.

Moggach, S.A., Oswald, I.D.H., 2020. Crystallography under high pressures. Struct. Bond. 185, 141–198. https://doi.org/10.1007/430_2020_70.

Nowell, H., Barnett, S.A., Christensen, K.E., Teat, S.J., Allan, D.R., 2012. I19, the small-molecule single-crystal diffraction beamline at Diamond Light Source. J Synchrotron Radiat. 19 (3), 435–441. https://doi.org/10.1107/S0909049512008801.

Oswald, I.D.H., Pulham, C.R., 2008. Co-crystallisation at high pressure - An additional tool for the preparation and study of co-crystals. CrystEngComm 10 (9), 1114–1116. https://doi.org/10.1039/b805591b.

Oswald, I.D.H., Urquhart, A.J., 2011. Polymorphism and polymerisation of acrylic and methacrylic acid at high pressure. CrystEngComm 13 (14), 4503–4507. https://doi.org/10.1039/c1ce05295k.

Paliwoda, D., Dziubek, K.F., Katrusiak, A., 2012. Imidazole hidden polar phase. Cryst. Growth Des. 12 (9), 4302–4305. https://doi.org/10.1021/cg300852t.

Piermarini, G.J., Block, S., Barnett, J.D., Forman, R.A., 1975. Calibration of pressure-dependence of R1 ruby fluorescence line to 195 kbar. J. Appl. Phys. 46 (6), 2774–2780. https://doi.org/10.1063/1.321957.

Rao, R., Sakuntala, T., Godwal, B.K., 2002. Evidence for high-pressure polymorphism in resorcinol 54108-54108. Phys. Rev. B 65 (5), 54108. https://doi.org/10.1103/PhysRevB.65.054108.

Reeves, M.G., Wood, P.A., Parsons, S., 2020. MrPIXEL : automated execution of pixel calculations via the mercury interface. J. Appl. Cryst. 53 (4), 1154–1162. https://doi.org/10.1107/s1600576720008444.

Rigaku, OD, 2021. *CrysAlis PRO*. Rigaku. Oxford Diffraction Ltd, Yarnton, Oxfordshire, England.

Safari, F., Katrusiak, A., 2021. High-pressure polymorphs nucleated and stabilized by rational doping under ambient conditions. J. Phys. Chem. C 125 (42), 23501–23509. https://doi.org/10.1021/ACS.JPCC.1C07297.

Sheldrick, G.M., 2008. SADABS, programs for scaling and absorption correction of area detector data. SADABS, Programs for Scaling and Absorption Correction of Area Detector Data. Published online:University of Göttingen: Göttingen, Germany-University of Göttingen: Göttingen, Germany.

Srirambhatla, V.K., Guo, R., Price, S.L., Florence, A.J., 2016. Isomorphous template induced crystallisation: a robust method for the targeted crystallisation of computationally predicted metastable polymorphs. Chem. Commun. 52 (46), 7384–7386. https://doi.org/10.1039/C6CC01710J.

Thakral, N.K., Thakral, S., Stephenson, G.A., Sedlock, R., Suryanarayanan, R., 2019. Compression-induced polymorphic transformation in tablets: role of shear stress and

development of mitigation strategies. J. Pharm. Sci. 108 (1), 476–484. https://doi.org/10.1016/j.xphs.2018.09.015.

Wildfong, P.L.D., Morris, K.R., Anderson, C.A., Short, S.M., 2007. Demonstration of a shear-based solid-state phase transformation in a small molecular organic system: chlorpropamide. J. Pharm. Sci. 96 (5), 1100–1113. https://doi.org/10.1002/jps.20920.

Wilson, C.J.G., Cervenka, T., Wood, P.A., Parsons, S., 2022. Behavior of occupied and void space in molecular crystal structures at high pressure. Cryst. Growth Des. 22 (4), 2328–2341. https://doi.org/10.1021/acs.cgd.1c01427.

Winter, G., 2010. xia2: an expert system for macromolecular crystallography data reduction. J. Appl. Cryst. 43 (1), 186–190. https://doi.org/10.1107/S0021889809045701.

Wishart, D.S., Feunang, Y.D., Guo, A.C., et al., 2018. DrugBank 5.0: a major update to the DrugBank database for 2018 Nucleic Acids Res. 46 (D1), D1074-D1082. doi: 10.1093/nar/gkx1037.